Stanford | SCHOOL OF EARTH, ENERGY & ENVIRONMENTAL SCIENCES

EMMA J. HARRISON, PH.D., POSTDOCTORAL FELLOW
DEPARTMENT OF GEOLOGICAL SCIENCES
SCHOOL OF EARTH, ENERGY AND ENVIRONMENTAL SCIENCES
STANFORD UNIVERSITY
450 SERRA MALL, BUILDING 320, STANFORD, CA 94305-2115, USA
E: EJHARRIS@UCSD.EDU T: 480.710.9649 F: 650.725.0979

April 7th, 2022

"Quantifying Rates of Landscape Unzipping" by Harrison et al. is a non-peer reviewed preprint manuscript submitted to EarthArXiv. The manuscript has been submitted to the journal JGR Earth Surface for peer review.

The manuscript authors, affliations, and their twitter handles are:

Emma J. Harrison, ejharris@ucsd.edu
Scripps Institution of Oceanography, University of California San Diego, La Jolla, CA, USA
Now at Geological Sciences, Stanford University, Stanford, CA, USA
@annelids4life

Jane K. Willenbring, willenbring@stanford.edu
Scripps Institution of Oceanography, University of California San Diego, La Jolla, CA, USA
Now at Geological Sciences, Stanford University, Stanford, CA, USA
@jkwillenbring

Brandon McElroy, bmcelroy@uwyo.edu
Department of Geology and Geophysics, University of Wyoming, Laramie, WY 82071, USA

Thank you,

Emma J. Harrison

Quantifying Rates of Landscape Unzipping

Emma J. Harrison[1*], Brandon McElroy[2], and Jane K. Willenbring[1]

[1] Geological Sciences, Stanford University, Stanford, CA 94305 USA
* Now at: Department of Oceanography, Dalhousie University, Halifax, Nova Scotia, B3H 4R2, Canada

[2] Department of Geology and Geophysics, University of Wyoming, Laramie, WY 82071, USA

Corresponding author: Emma Harrison (ejharris@ucsd.edu)

Key Points:

- Propagation rates of morphologic features determined by nuclide concentration gradients along a horizontal transect
- Uplift rate of the Florida panhandle estimated between 0.027 and 0.038 mm/y from a nuclide depth profile
- Changes in climate over the Quaternary likely drove variable growth rates of seepage valleys along the Apalachicola River

Abstract

Measuring rates of valley head migration and determining the timing of canyon-opening are insightful for the evolution of planetary surfaces. Spatial gradients of *in situ*-produced cosmogenic nuclide concentrations along horizontal transects provide a framework for assessing the migration of valley networks and similar topographic features. We developed a new derivation for valley head retreat rates from the concentration of *in situ* produced cosmogenic radionuclides in valley walls. The retreat rate is inversely proportional to the magnitude of the spatial concentration gradient and proportional to local nuclide production rates. By solving for a spatial gradient in concentration along a valley parallel transect, we created an expression for the explicit determination of valley head retreat, which we refer to herein as unzipping. We applied this expression to a seepage-derived drainage network developing along the Apalachicola River, Florida, USA. Sample concentrations along a valley margin transect varied systematically from 2.9×10^5 atoms/g to 3.5×10^5 atoms/g resulting in a gradient of 160 atoms/g/m, and from this value a valley head retreat rate of 0.025 m/y was found. The discrepancy between overall network age and current rates of valley head migration suggests intermittent network growth which is consistent with glacial-interglacial precipitation variations during the Pleistocene. This method can be applied to a wide range of Earth-surface environments. For the ^{10}Be system, this method should be sensitive to unzipping rates bounded between 10^{-6} m/y and 10^{0} m/y.

Plain Language Summary

The pace at which landforms develop is an important control on many biological, chemical, and physical processes operating at Earth's surface. Rates of landscape change are often quantified by measuring the accumulation of cosmogenic radio nuclides in near-surface Earth materials, as an indicator of the erosion rate and age of landforms. In this study, we advance a method for querying the rate of horizontal topographic changes, such as valley growth or ice margin retreat, by sampling material in a horizontal transect and observing patterns in the nuclide concentrations in a spatial gradient. We present the results of numerical modeling that describe the limits of this approach due to the rate and consistency of ongoing landscape evolution processes. We present the first empirical data on the growth rate of a well-studied seepage channel network in Florida, which suggests that the time-averaged channel advance rate is 0.025 m/y. Furthermore, our measurements indicate that the age of the incising plateau surface is between 2 and 2.5 My and that the regional uplift rate is between 27 and 38 m/My.

1 Introduction

One of the primary ways of understanding the dynamics and kinematics of Earth's surface is by querying rates of topographic change. Of a host of tools used to accomplish this, the accumulation of cosmogenic radionuclides near the surface in eroding landscapes has been used to make estimates of local denudation rates on rock faces (Lal, 1991; Nishiizumi et al., 1991), conversion of bedrock to soil (Heimsath et al., 1997), ages of fluvial strath terraces (Repka et al., 1997; Reusser et al., 2004), the evolution of passive margin escarpments (Heimsath et al., 1999; Bierman and Caffee, 2001; Vanacker et al., 2007), and basin-averaged erosion rates (Bierman and Stieg, 1996; Granger et al., 1996). Brown et al. (1995), Granger et al. (1996), and Bierman and Stieg (1996) propose that sediments in channels represent a mixed sample from the eroding hillslopes of the basins that they drain. With the appropriate caveats, von Blankenburg (2006) summarized this idea as the "let nature do the averaging" approach.

Here, we explore spatial gradients in nuclide concentration created by the serial exposure of previously buried surfaces as a direct method for obtaining the axis-parallel migration rates of morphologic features. In some cases, measuring the spatial patterns in nuclide concentration across a surface can provide additional estimates of topographic evolution that are more localized in their interpretation than basin-averaged methods. Measuring spatial variations in calculated ages is a similar approach and has been demonstrated in the contexts of timing of ice margin retreat during deglaciation (Balco et al., 2009; Briner et al., 2009; Ward et al., 2009), knickpoint incision (Jakica et al., 2011; Jansen et al., 2011; Mackey et al., 2014; Valla et al., 2010), and slip rates along exposed faults (Mitchell et al., 2001; Bendetti et al., 2002; Polumbo et al., 2004). These authors effectively removed issues associated with inheritance by excluding or specifically testing sample localities for inherited nuclide concentrations. Where this strategy cannot be successfully employed, inheritance adds uncertainty to calculating ages. The uncertainty associated with inheritance can be minimized if it is appropriate to assume that concentrations of cosmogenic nuclides are constant in space prior to exposure.

We further developed these methods, showing that it is not necessary to first measure ages of surfaces to calculate the rates of lateral migration of topographic features. Specifically, the sequential exposure of valley walls as the topography develops should be explicitly related to spatial gradients in cosmogenic nuclide concentrations along the valley axis given constraints on production and inheritance. Although other studies have used horizontal CRN concentration gradients to determine cliff retreat rates (Hurst et al., 2017; Swirad et al., 2020), here, we show that it may also be applied to laterally migrating topographic features, e.g., the opening of valleys, head cutting in sapping canyons, retreating ice sheets, or migrating knickpoints.

In the following we advance the existing theory for calculating rates of horizontally migrating topography using an example application in an expanding valley network. The network, growing through groundwater seepage, has been modeled in detail by Lobkovsky et al. (2007), Abrams et al. (2009), and Petroff et al. (2011). This work supplies the first empirical data on the kinematics of network growth and provides another constraint for these physical models. We discuss the results in the field area context with respect to exposure history and explore the limitations of this method by modeling concentration gradients produced under theoretical network growth and decay scenarios. Furthermore, the results of the nuclide measurements were modeled to apply age constraints to the uplift of the plateau region where the channel network is located.

2.0 Theory

The governing differential equation for the accumulation of *in situ* produced cosmogenic isotopes in Earth surface materials is:

$$\frac{\partial N(x,z,t)}{\partial t} = P_0(x,t)e^{-(z/\Lambda)} - N(x,z,t)\lambda \qquad (1)$$

where N is the nuclide concentration with units of atoms/g, as a function of horizontal space, x, and vertical space, z, with units m, and time, t with units y, λ is the disintegration constant for the nuclide with units 1/y, P_0 is the surface production rate as a function of x and t with units atoms/g/y, and Λ is the absorption mean free path with units g/cm^2 (Lal, 1988; Lal, 1991). Equation 1 is slightly modified from the version of Lal (1988) for the purposes of explicitly accounting for horizontal concentration gradients. This can be accomplished by applying the chain rule to the first term in Eq 1.

$$\frac{\partial N(x,z,t)}{\partial t} = \frac{\partial N(x,z,t)}{\partial x}\frac{\partial x}{\partial t} = \frac{\partial N(x,z,t)}{\partial x}V \qquad (2)$$

where V represents the valley head migration rate with units m/y. It is appropriate to interpret this generally as the rate of propagation of horizontal concentration or morphologic contours and more specifically in this case as the migration rate of a steady topographic form. We refer to this consistent migration as unzipping. Propagation rates of topographic features are related to accumulation and spatial gradients in concentration (units of atoms/g/m) by:

$$V = \left(P_0(x,t)e^{-(z/\Lambda)} - N(x,z,t)\lambda\right)\left(\frac{\partial N(x,t)}{\partial x}\right)^{-1} \tag{3}$$

For fairly young features with low concentrations and negligible mass loss after unzipping, this reduces to:

$$V = P_0(x,t)\left(\frac{\partial N(x,z,t)}{\partial x}\right)^{-1} \tag{4}$$

Equations 3 and 4 can be used to query a variety of evolving landscapes where approximately steady migration of morphologic entities is suspected from field observations. This theory can be equally applied to the unzipping of a bedrock substrate, as in a case of badland canyon formation or strath terrace creation due to knickpoint migration, or to the unzipping of soil mantled landscapes, as in a case of channel initiation in hilly topography. This calculation is specifically relevant to horizontal migration and assumes that differences in hillslope diffusional response along the sampled transect are minimal.

When materials are buried at depths much greater than 1 m, they are shielded from spallation production of cosmogenic nuclides. Depending on the nuclide system, concentrations in buried materials are understood to be inherited from previous exposure such as original deposition. Typically, the mean concentration of a shielded sample, or samples, is subtracted from concentrations of surface samples to determine the concentration accumulated during recent exposure rather than prior exposure. Our approach does not require a subtraction of the inherited component, but it does require the validity of either of two assumptions: 1) that the inherited nuclide concentration is constant over the area where the gradient is measured, or 2) that the inherited component is small compared to the total concentration difference across space over which a gradient is measured. If the inherited component proportion is large, i.e., equal to the change through time over a spatial gradient, then the analytical and measurement uncertainties would likely be as large as any variability in the inheritance and would overwhelm any signal of spatial variation that might otherwise be detected. The extent and limits to possible future applications are fully explored in the discussion that follows.

3.0 Example Application

3.1 Sampling Site

We applied this theory to a young and rapidly growing channel network, Beaverdam Creek, adjacent to the Apalachicola River in Florida, USA in the Apalachicola Bluffs and Ravines Nature Preserve (Fig. 1). The flat uplands are nearly barren of large, woody vegetation (Fig. 2) and do not support overland flow because of high infiltration rates (up to 300 mm per hour) (Schumm et al., 1995). Springs emerge at the tips of the channels, and the channel growth proceeds by undercutting and headwall collapse at the spring site (e.g., Dunne, 1988). Excavation at spring locations indicated there is no obvious stratigraphic control on their vertical positions. This observation was also reported by Schumm and others (1995) for nearby regions. In the absence of a lithologic control, the position of the springs is set by the height of the phreatic water table. Abrams et al. (2009) performed a ground penetrating radar survey in this area, finding that the retreat rate for channel tips was proportional to the groundwater flux to the channel heads. The ravines cut unlithified Plio-Pleistocene sandy strata, the Citronelle Fm. (Fig. 1), with major constituents of unconsolidated coarse detrital sands and minor constituents of unconsolidated detrital silt and clay (Schmidt, 1985). The upstream extents of valleys terminate with slopes that rise up to the surrounding upland at angles near repose and are locally termed steepheads.

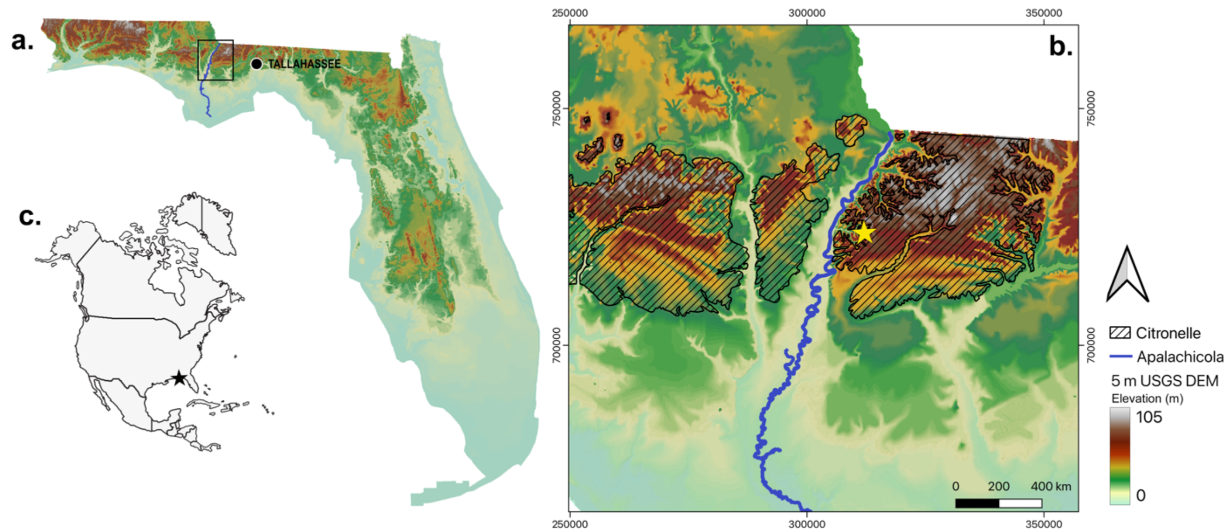

Fig. 1 Regional context of the study region. a.) Digital elevation data for the state of Florida with the study area identified by a black box. b.) Context for the study site showing the main Appalachicola River channel and the Citronelle Fm. The channel network extending east from the main channel and incising the Citronelle Fm contains the channel network investigated in this case study. A star marks the location of the study area (segment A). Coordinates in WGS 84 / UTM zone 16N c.) A map of North America showing regional context for the study area.

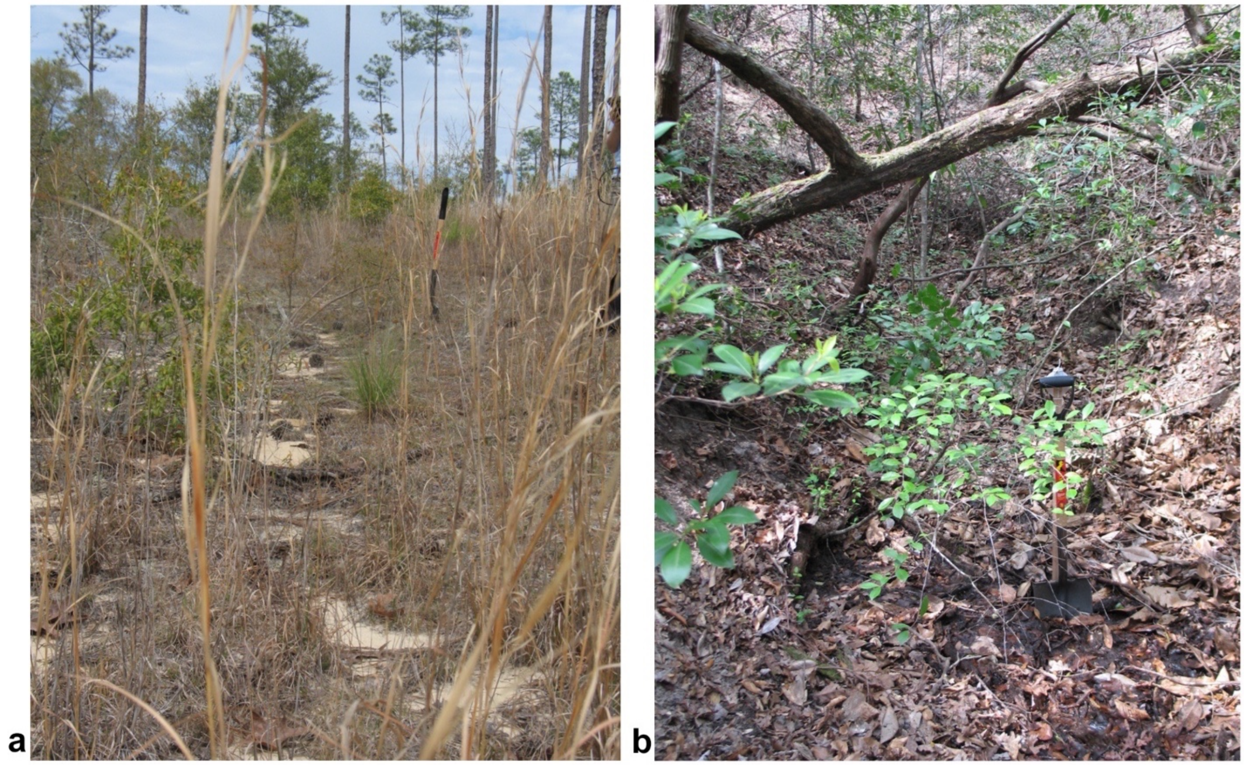

Fig. 2. a.) Field images of the study area showing the flat upland surface and b.) the base of the steephead looking upslope. Longleaf pines and wiregrass dominate in the uplands. Beach, magnolia and abundant woody understory plants are found within the steepheads (Kwit et al., 1998).

Channel segment A, a small branch of Beaverdam Creek, (Fig. 3) is extending through the action of sapping associated with groundwater springs located at its steephead. The width of the valley is nearly constant along its length, consistent with the theory that channel widening driven by erosion of the valley walls is minimal compared to the erosion associated with extending the length of the valley. However, as the wall materials consist largely of unconsolidated materials, valley flanks can maintain angles near repose despite a range in erosion rates (Zavala et al., 2021). Eq. 4 can be used to estimate the rate of migration of the steephead based on the *in situ* accumulation of ^{10}Be in quartz sand only where valley flank erosion plays a minor role. However, patterns in the spatial gradient of nuclide concentrations can be useful in determining whether this assumptions holds for a given study area. This is further explored in section 4.2.

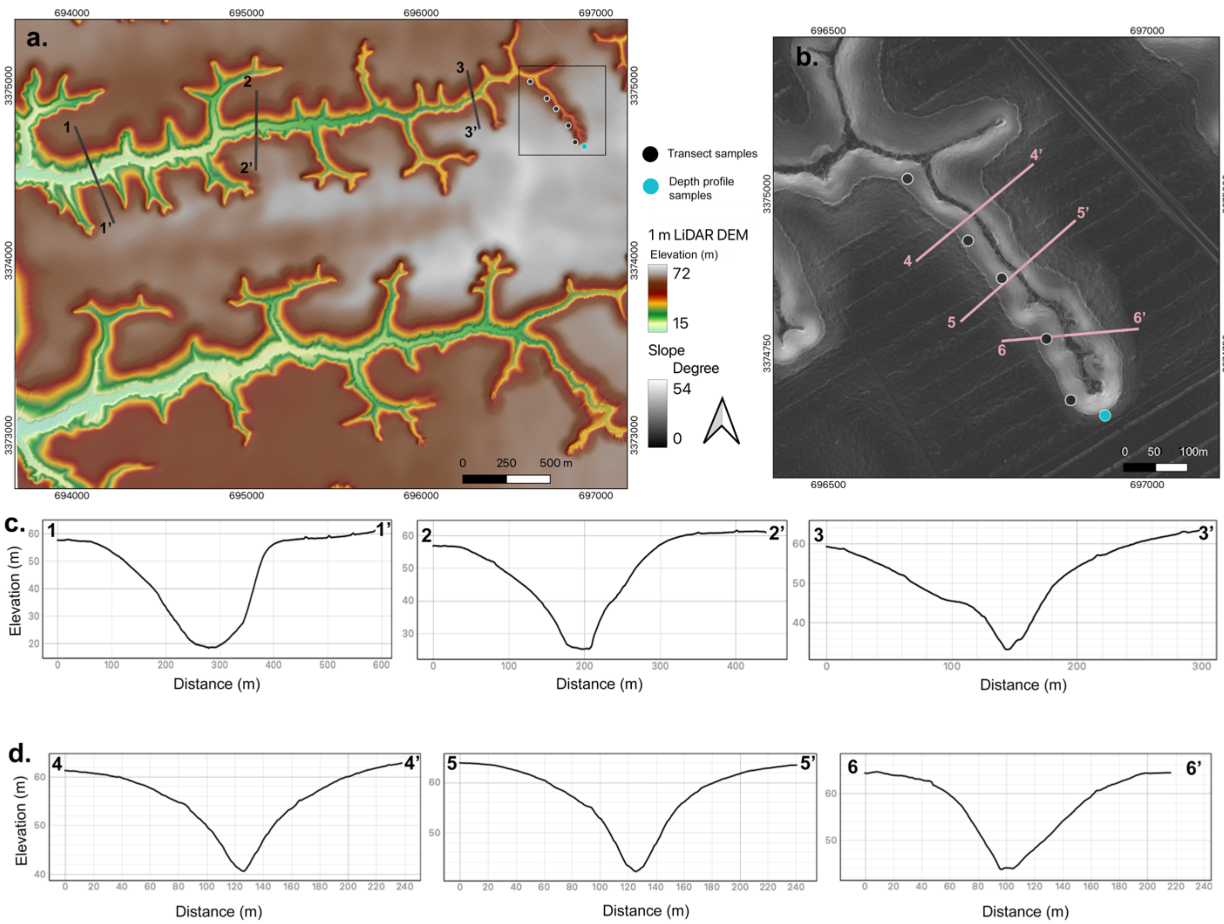

Fig. 3. a.) DEM of Beaverdam Creek, in the Apalachicola Bluffs and Ravines Nature Preserve. Black lines correspond to cross-sections in (c.) and are numbered. Black square shows the location of segment A and the sampling locations for this study. Coordinates in WGS 84 / UTM zone 16N b.) A slope map of segment A showing the locations of the sample sites and the cross-sections corresponding to (d.) c.) cross-sections from the Beaverdam Creek network. Note the scale changes in the x-axis. d.) cross-sections from segment A. Slope angles are near repose (30 to 35 degrees) to typical depths of 15 m to 20 m. Ravine geometry includes valleys that are 80 m

to 100 m wide at their upper contour, and valley bottoms are generally flat with widths around 10 m.

3.2 Methods

We collected six samples in a vertical depth profile to constrain the age and uplift rate of the plateau surface into which the stream network is incising. To constrain the valley migration rate, we collected five samples along an axial transect at approximately equal elevations. These samples were collected from the hillslopes at an approximately constant elevation of 60 meters.

3.2.1 Depth profile

We determined the depth of the mixed layer by measuring a vertical profile of samples near the terminus of the river segment A (Fig. 3). The vertical profile is comprised of a total of six samples to a depth of 2 m. An additional sample was taken at a depth of 5 m below the upland surface by excavating horizontally into a steephead with a vertical face from sediments partially indurated by authigenic kaolinite. This horizontal distance was as far as could be reached behind the face with an arm and a trowel (ca. 1 m). Five meters is a sufficient depth for the sample to represent materials shielded by burial and should be a limit for inheritance during primary deposition of the sands. The accumulation of ^{10}Be, $N_{total}(z,t)$ (atoms/g), in an eroding surface is a function of the inherited concentration, N_{inh} (atoms/g), and the production of nuclides following the deposition or exposure of the surface:

$$N_{total}(z,t) = N_{inh} + \sum_i \frac{P(z)}{\lambda+\frac{\rho E}{\Lambda}} e^{-(\rho(z_0-Et)/\Lambda)} \left(1 - e^{-\left(\lambda+\frac{\rho E}{\Lambda}\right)t}\right) \qquad (5)$$

where ρ is the sediment density with units of g/cm^3, λ is the disintegration constant for the nuclide with units 1/y, Λ is the absorption mean free path with units m, and $P(z)$ is a production rate dependent on depth, z (units cm), given by:

$$P(z) = P_0 e^{-\frac{z\rho}{\Lambda}} \qquad (6)$$

We used a sediment density of 1.6 g/cm^3 for the sandy material, an absorption length Λ of 160 g/cm^2, a disintegration constant λ of 5x10^{-7}, and a surface ^{10}Be production rate of 4.1 atoms/g/y, determined using the online calculator formerly known as CRONUS-Earth online calculator (Balco et al., 2008), a topographic shielding parameter of 0.999, and a regional erosion rate of 10 mm/ky.

We modeled the unknown parameters in equations 5 and 6, *E,* erosion rate in cm/y, and *t,* exposure age in y, with a Bayesian inversion of the ^{10}Be-depth profile (Laloy, et al. 2017). The prior distributions were generated with a Markov chain Monte Carlo (MCMC) simulation. The prior distribution for *E* was assumed to be gaussian with a mean of 20 mm/ky and a standard deviation of 20 mm/ky. The upper bound of 40 mm/ky anticipates modest erosion on the flat, upland surface. Priors for the exposure age, *t*, were modeled with a uniform distribution between 0 and 4 My, based on the presumed Plio-Pleistocene deposition age (Schumm et al. 1995). We considered the inherited concentration as an additional parameter in the model, with a uniform prior distribution bounded by the analytical uncertainty on the concentration measured in the shielded sample collected at 5 m depth.

We used code from Laloy et al. (2017) to perform the inversion and to generate the MCMC samples. This program implements the DREAM$_{(zs)}$ algorithm in generating the posterior samples (ter Braak and Vrugt, 2008; Vrugt et al. 2009; Laloy and Vrugt, 2012). The package does not assume that model errors are fixed to observation errors and provides an error estimate combining both error sources. Five MCMC chains with a burn-in at 2500 (an estimated number of iterations needed to enter the high-probability region), a value of 1 for thinning (the default value), and 150,000 iterations were used to generate the samples. Trace plots indicated that the samples mixed well and were not autocorrelated after burn-in.

3.2.2 Zipper transect

To quantify the spatial gradient in nuclide accumulation along the margin of segment A, a series of five samples were collected from a 460 m long transect of the southwestern slope of a valley axis (Fig. 3). To avoid collecting materials that have seen significant accumulation of nuclides prior to the unzipping event, samples were collected on valley slopes approximately 5 m below the upland surface, well below the zone of spallogenic nuclide production prior to incision. Because of dense vegetation within the valleys, complete vertical mixing of surface and subsurface materials was assumed. In an effort to collect samples from the middle portions of the surface mixing zone, samples were taken from 0.3 m beneath the ground surface. We used the surface production rate (4.1 atoms/g/y) assuming complete mixing at 0.3 m depth and that the profile is in steady state. The values applied for the disintegration rate, bulk density, and absorption path length are the same as used in the depth profile analysis.

By using equations 3 and 4 to derive the velocity retreat rate, we make the simplifying assumption that denudation processes on the valley walls have not lowered the CRN concentrations in the samples. If the exposure time for downstream samples is long relative to the upstream sites, surface processes may have lowered the CRN concentrations in the samples downstream. Therefore, this method is best applied in cases where unzipping is fast relative to exposure time. This is discussed further in section 4.2. Other methodological assumptions inherent to these equations are a constant nuclide production rate over the relevant time frame and negligible muon production.

3.2.3 ^{10}Be measurements

Beryllium extraction was performed at the University of Pennsylvania cosmogenic lab between April and May of 2011. The chemical blank ratio ($^{10}Be/^{9}Be$) run with this sample was $4x10^{-15}$; $3.4x10^{3}$ atoms of ^{10}Be were added to the samples via the chemical blank. The quartz samples were spiked with 250 µl of a 10^{-3} g/g ^{9}Be solution from CEREGE, Aix-en-Provence, France, before dissolution. An adaption of the Kohl and Nishiizumi (1992) chemical procedure was used for quartz purification and Be extraction. The $^{10}Be/^{9}Be$ ratio was measured via AMS at PRIME Lab at Purdue University during January of 2012.

3.3 Results

3.3.1 Depth profile

The samples collected from a vertical profile below the upland surface at the valley head varied in ^{10}Be concentration from $9.9x10^{4}$ atoms/g to $4.1x10^{5}$ atoms/g with analytical errors around 1% to 2.7% (Table 1). The profile (Table 1 & Fig. 5) showed vertical mixing between ~0.5 and 1 m below the surface evidenced by a roughly constant concentration profile. Below about 1 m, ^{10}Be concentration decreased exponentially. Using the vertical profile concentrations as input to the Laloy et al. (2017) algorithm provided an estimated duration over which the upland had been accumulating nuclides *in situ* and a rate of mass loss from the upland surface. Model results are shown in Fig. 4. The erosion rate was well resolved with a clear mode at 10 mm/ky. Values for the first and third quantile were 10.2 and 11 mm/ky respectively. The exposure age posterior distribution had a mode at 2.5 My and was strongly skewed towards ages < 2.5 My. The first and third quantile values were 1.7 My and 2.5 My respectively, and the median age was 2.1 My. Minimum and maximum ages for the distribution were 150 ky and 3.3 My.

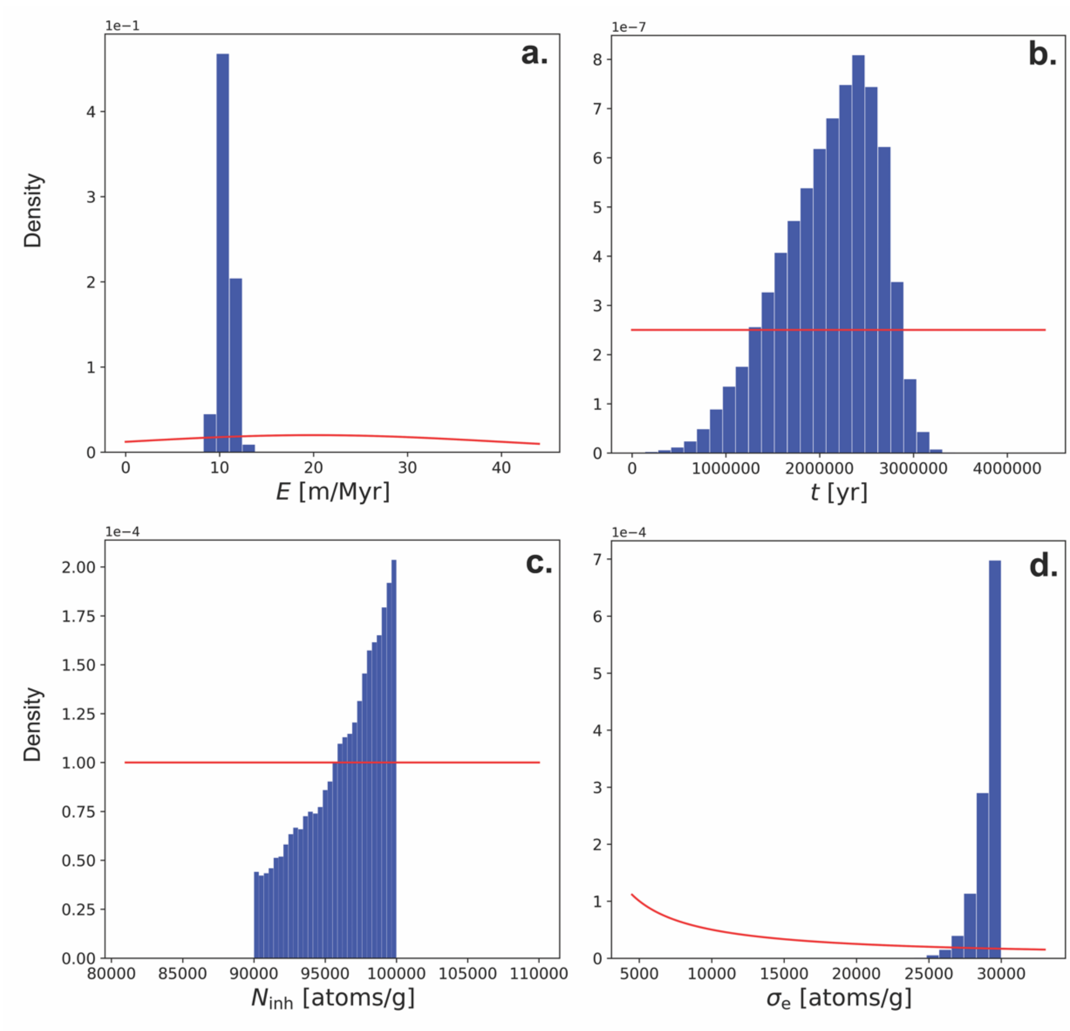

Fig. 4 Results from a Bayesian inversion of a ^{10}Be depth profile collected from 0 to 5 m depth at the terminus of the studied river segment. Probability density plots for the unknown parameters in equation 5 are presented along with estimates of the model error. Blue bars represent the posterior probability density and red lines indicate the prior probability density functions a.) regional erosion rate *E*. b.) surface age *t*. c.) inherited nuclide concentration N_{inh}. d.) model error σ_e (Laloy et al., 2017).

3.3.2 Zipper transect

The series of samples taken in a transect along the valley had concentration values that ranged between $2.9\text{x}10^5$ and $3.5\text{x}10^5$ atoms/g with analytical errors between 1% and 2% (Table 1). Concentrations decreased linearly with distance from the downstream end of the valley toward the steephead (Fig. 5). The slope of the best-fit line of concentration plotted against distance is the magnitude of the spatial gradient of concentration. It was found to be 160 atoms/g/m with a Pearson correlation coefficient of 0.90 and a p-value of 0.013. At the 5% confidence level we rejected the null hypothesis that the trend was spurious and used the concentration gradient to determine the rate of propagation of the valley head into the un-dissected regions of the upland surface.

Table 1. Cosmogenic ^{10}Be Samples & Concentrations

Sample	Easting [m]	Northing [m]	Depth [cm]	Mass[1] [g]	Concentration [atoms/g]	Uncertainty [%]
Vertical Profile Samples						
FLA-10-BDC-06	696934	3374653	0	43.1	4.06E+05	2.1
FLA-10-BDC-05	696934	3374653	45	43.2	3.88E+05	2.1
FLA-10-BDC-04	696934	3374653	95	42.5	3.84E+05	1.6
FLA-10-BDC-03	696934	3374653	150	55.6	2.73E+05	1.6
FLA-10-BDC-02	696934	3374653	170	54.8	2.15E+05	1.6
FLA-10-BDC-01	696934	3374653	192	55.7	1.86E+05	1.7
BDC-07-SHLD-01	696198	3375451	5.00	50.6	9.90E+04	2.7
Zipper Transect Samples						
FLA-10-BDC-16	696624	3375024	30	32.7	3.50E+05	1.6
FLA-10-BDC-17	696719	3374927	30	36.5	3.35E+05	1.6
FLA-10-BDC-18	696772	3374868	30	38.9	3.07E+05	1.7
FLA-10-BDC-19	696842	3374773	30	34.6	2.87E+05	1.8
FLA-10-BDC-20	696880	3374677	30	54.4	2.90E+05	1.5

[1] Mass of quartz sample analyzed. Most samples were approximately 1-2 kg of material. Sample elevations are all 60±10 m.

In this case, the product of N ($4.0\text{x}10^5$ atoms/g) and λ ($5.0\text{x}10^{-7}$/y) is 0.205 atoms/g/y. The production and decay values were combined with the gradient of 160 atoms/g/m by applying them to equation 3, giving a result of V=0.025 m/y. The decay rate is small, even for the largest measured concentration, and therefore, the simplified equation 4 produces the same result.

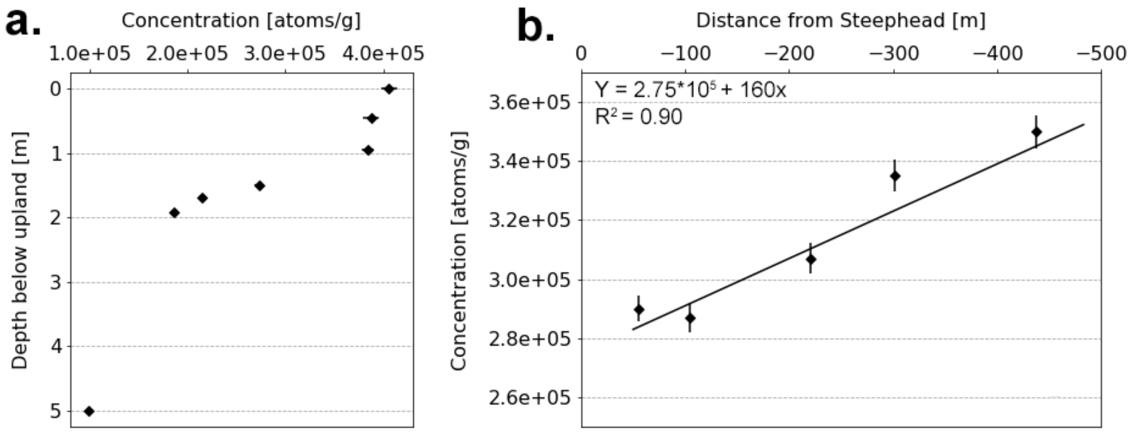

Fig. 5. Concentrations profiles of ^{10}Be at sample locations in Fig. 3 and Table 1. Depth profile (a) shows a zone of mixing between 0.5 and 1 m depth, followed by an exponential decrease in concentration. The sample collected at five m depth was taken from a separate location and constrains the local inheritance of ^{10}Be. Data were used to produce a best fit model for the age and erosion rate of the surface (Laloy et al. 2017). Zipper profile (b) shows the concentration change along the length of the valley segment A (Fig. 3). A linear least-squares regression gives a slope of 160 atoms/g/m and can explain 90% of the variance of the concentration.

4.0 Discussion

4.1 Timing and rate of network development

We used the spatial gradient in *in situ* produced cosmogenic nuclides from segment A to interpret the growth rate of the Beaverdam Creek network into unconsolidated sediments along the Apalachicola River of Florida. From the ^{10}Be depth profile, we found that the overall age of the surface into which the channels are cutting is likely between 2 and 2.5 My. Based on the spatial gradient of 160 atoms/g/y, we calculated the rate of unzipping at the valley head to be 0.025 m/y.

The combination of the age of the upland surface and the rate of channel growth implies an overall channel length of ~50 km assuming steady growth. The actual modern length of Beaverdam Creek is around 4 km, which would imply a steady growth rate of ~0.002 m/y based on the age of the upland surface. This implies that either: 1) a significant portion of the channel length has been eroded by the Apalachicola River, 2) the rate of valley head migration has varied through time, 3) lateral valley flank erosion has lowered the ^{10}Be concentration, which results in an overestimation of valley head retreat rates (section 4.2), or 4) the seepage valley network has grown at a constant rate, 0.025 m/y, over a period of only 160 ky as necessary to create the observed 4 km of length from its confluence with the Apalachicola River to its upstream most channel tip.

We suspect that valley growth rates have fluctuated over times due to secular variations in precipitation over the Pleistocene and Holocene. Abrams and others (2009) presented a process model for the growth of this channel network by sapping of valley steepheads due to groundwater seepage as investigated by Schumm and others (1995). The basis of their model is the combination of Darcy flow with drainage of evolving groundwater catchments. They found the network along the Apalachicola River satisfies the proposal of Howard (1988) that valley heads might migrate as a function of their contributing groundwater drainage area. Because a water table is capable of responding on timescales very short relative to changes in a sapping channel network, Abrams and others (2009) constrain modern channel-tip growth velocities and iterate backward to evolve the current network in reverse through time. Their model predicts a time-averaged growth rate of 0.0053 m/y and a slower modern growth rate of 0.0005 m/y. The gradient in nuclide concentrations from the channel tip to its junction with the main channel implies a growth rate four-times greater than the time-integrated velocity given by Abrams et al. (2009).

Changes in precipitation through time would cause variations in the discharge of groundwater at springs. Consistent with the Howard (1988) and Abrams and others (2009) models, lower total rainfall would have the consequence of slowing rates of network evolution associated with decreased seepage. Laîné and others (2009) report that glacial-interglacial or even millennial climate fluctuations including precipitation could have been substantial. This is also supported by local and regional palynology in the eastern U.S. (Grimm, et al., 1993; Jackson et al., 2000) as well as regional speleothem records (Alvarez Zarikian et al., 2005; Van Beynen et al., 2008). As a result of Quaternary fluctuations in rainfall, total groundwater discharge could have caused intermittent termination or reduced rates of migration of valley steepheads. The observed near-linear trend of ^{10}Be concentrations along the 500 m transect of segment A indicates that the retreat rate has been approximately steady throughout the time that this segment has been incised, suggesting that fluctuations in rainfall and associated channel head migration occurred prior to the opening of this segment of the channel network.

We also cannot discount the hypothesis that the Beaverdam Creek network is ~160 ky old, and has been growing at a constant rate since inception. The evolution of this site is linked to the fluvial dynamics of the Apalachicola River. Evidence for drainage reorganization in the Apalachicola network includes channel morphology and χ mapping (Johnson, 1907; Willett et al., 2014) and the distribution of freshwater species (Sepkoski and Rex, 1974). Although drainage reorganization in this basin lacks age constraints, it is possible that knickpoint migration in the Appalachicola initiated the headward retreat of what is now Beaverdam Creek. This interpretation supports the linear pattern in ^{10}Be accumulation along the valley flank, which suggests that segment A formed at a constant, rapid rate (Fig. 5). This 500-meter long segment of river would have formed in ~20,000 years according to the spatial gradient in nuclide concentrations. The difference in nuclide concentration between the first and last transect samples is $6x10^4$ atoms/g requiring ~15,000 years of nuclide accumulation at a production rate of 4.1 atoms/g/y. Correcting the zipper transect samples for the inheritance measured in the 5 m deep sample from the depth profile and deriving exposure ages for the samples with the online calculator formerly known as CRONUS-Earth online calculator, we find that segment A began forming ~25 ky ago, in fitting with an overall river network age of 160 ky. In support of this theory, the tributary to the south (Fig. 3a), which joins the Apalachicola River downstream of Beaverdam Creek, has migrated a little further upstream than the river segment studied here.

4.2 Effects of exposure history on the zipper model

The exposure history of the valley flank will determine the spatial pattern in nuclide accumulation. We numerically modeled the impact of different exposure histories, including a non-steady unzipping rate, erosion of the valley walls after unzipping, and stability of the channel network after unzipping. In each scenario, we set the concentration of nuclides at the channel tip (Distance=0 in Fig. 6&7) equal to the measured nuclide inheritance (10^5 atoms/g) and the exposure age to zero. In one set of scenarios, we imposed patterns in the valley-parallel channel growth rate, under the uniform condition of no valley-perpendicular erosion. We calculated nuclide concentrations using equation 6 based on the exposure age of the valley wall. Fig. 6 shows the spatial patterns derived from a fast then slow unzipping, a pause during channel growth, and a pause after channel growth.

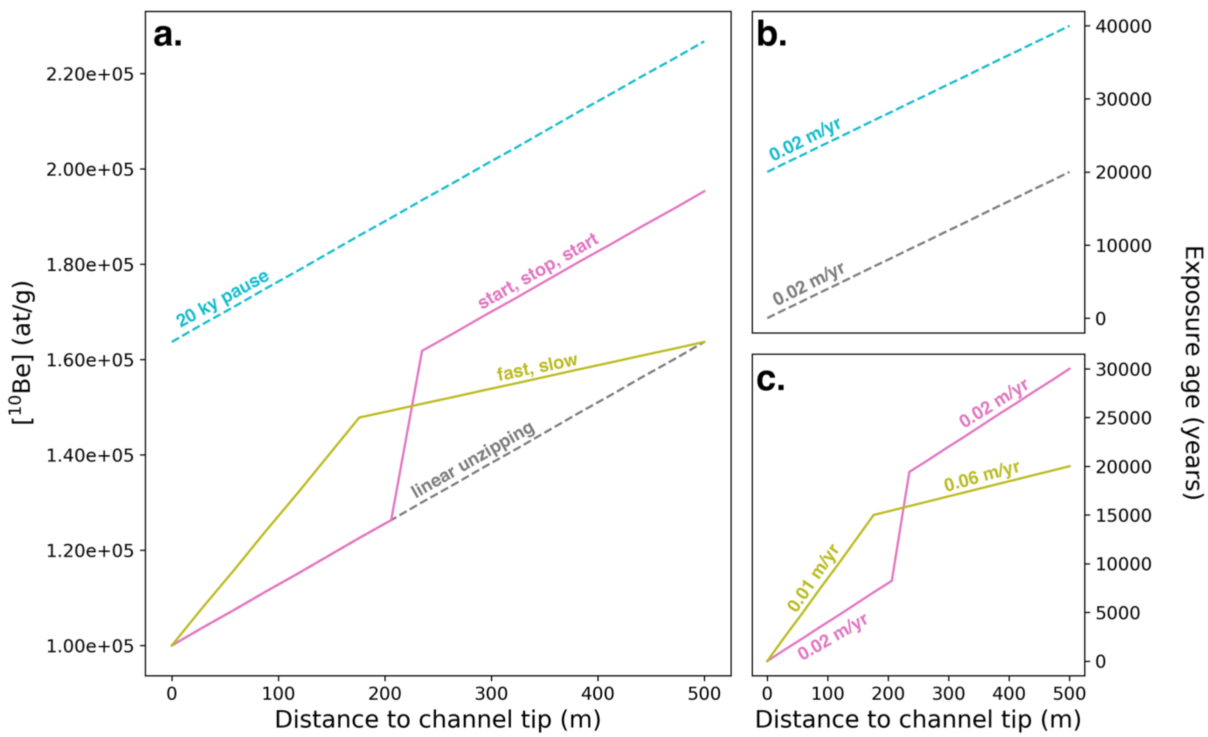

Fig. 6. a.) Concentrations of ^{10}Be along the valley axis from the channel junction with the main network (500 m) to the tip of the channel segment (0 m) for non-steady unzipping rates. b/c. show the channel growth rate and exposure age along the valley axis as the channel tip propagates. Four scenarios are shown: a linear growth rate (grey dashed line), linear growth followed by a 20 ky pause in network growth (cyan dashed line), constant growth interrupted by a 10 ky pause (pink line), and rapid growth replaced by slow growth (olive green line).

Analytical and numerical models of horizontally migrating valleys predict widening of the valley floor and greater topographic relaxation with increasing distance from the channel head (Pelletier and Taylor Perron, 2012; Perron and Hamon, 2012). The relative elapsed time for base level adjustment results in a pattern of increasing erosion rate with proximity to the steep head – which could produce a pattern of decreasing ^{10}Be concentrations unrelated to channel migration. In Fig.

7, we explored scenarios of valley-perpendicular erosion occurring along with channel incision. Again, we set the concentration of nuclides at the channel tip equal to the measured nuclide inheritance (10^5 atoms/g) and the exposure age to zero. We imposed a steady channel formation rate, and varied the erosion rate at valley-perpendicular positions along the channel length. In the modeled results, the blue dashed line constrains a no-erosion scenario. Green and orange dashed lines show spatially uniform but elevated rates of valley wall backwearing. Solid lines represent a linear increase in valley-perpendicular erosion toward the incising tip.

The model results show the concentration of ^{10}Be nuclides in valley wall positions along the channel axis. In the case of no valley-perpendicular erosion the nuclide concentrations along the valley axis decrease linearly towards the incising channel tip. Erosion of the valley flank produces non-linear patterns in nuclide concentration gradients. However, the degree of differentiation between the modeled scenarios depends strongly on the rate of channel formation. If the channel forms quickly (e.g., Fig. 7a) the nuclide concentrations are similar regardless of the scenario conditions. Over longer timescales, valley-perpindicular erosion produces pronounced non-linearity in the along-axis nuclide concentration gradient (Fig. 7b/c).

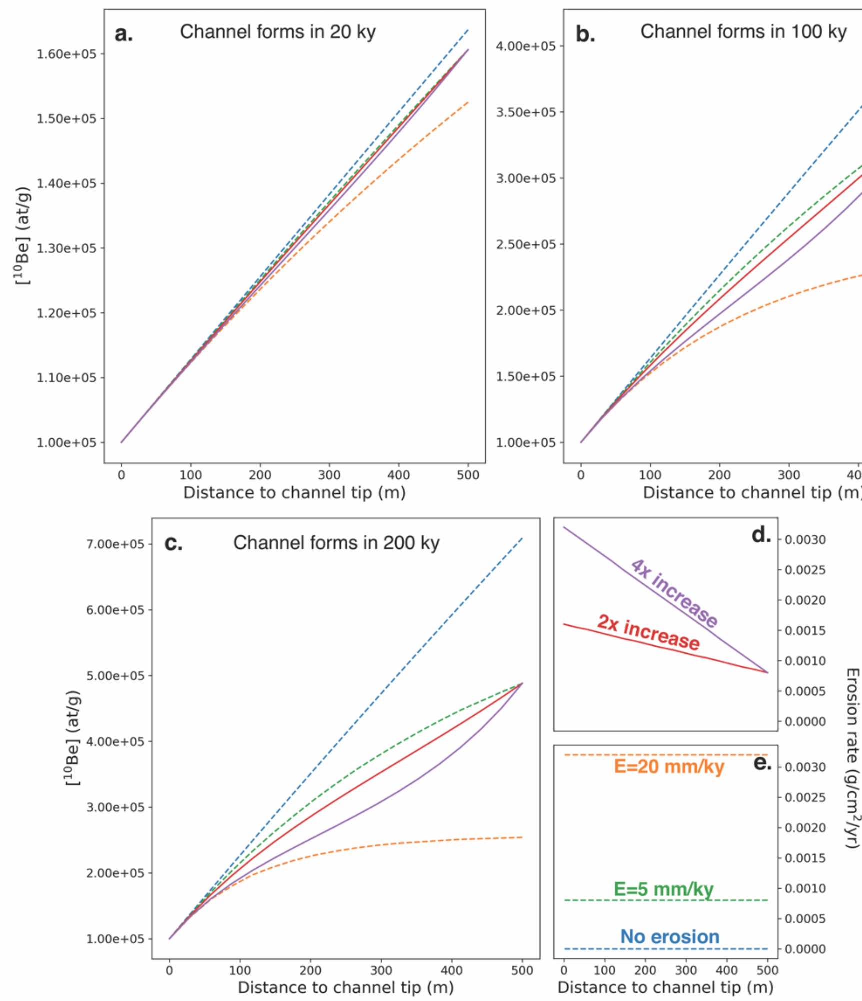

Fig. 7. a./b./c.) Concentrations of ^{10}Be along the valley axis from the junction with the main stem (500 m) to the tip of the channel segment (0 m) including erosion of valley flanks (or walls) after unzipping. d./e.) showt he valley-perpendicular hillslope erosion rate at positions along the valley axis after the channel has been established. Five scenarios are shown: no erosion (blue dashed line), spatially uniform but elevated erosion rates (orange and green dashed lines), a doubling of erosion from the junction to the channel tip (red line), and a quadrupling of erosion from the junction to the channel tip (purple line).

Our estimation of a 25 ky age for channel segment A suggests that we cannot reject the hypothesis that the nuclide concentration pattern we observe is influenced by valley flank erosion. However, we can check the assumption of no erosion by calculating the apparent erosion rate from the measured nuclide concentrations. In the case study presented here, the ^{10}Be concentrations ($>10^5$ atoms/g) obtained for the longitudinal transect preclude rapid hillslope erosion even if an inheritance of $\sim 10^5$ atoms/g is assumed. Measured concentrations require valley wall erosion rates $<10^{-5}$ m/y, an a posteriori demonstration that the negligible erosion assumption holds.

4.3 Constraints on uplift of Northern Florida

Data presented here were produced for an area above the Alum Bluff at the edge of the Tallahassee Hills adjacent to the Cody Escarpment. Concentrations of *in situ* produced ^{10}Be from the depth profile at our application site have an interquartile range of 1.7 My and 2.5 My with a median at 2.1 My and an elevation of 67 m. Because the depositional environment of the Citronelle Fm. and adjacent sands is interpreted to be deltaic to shallow marine from progradation of the Apalachicola Delta (Schmidt, 1985), this amount of uplift requires overall relative uplift rates between 0.027 and 0.038 mm/y since the Mid-Pleistocene, taking the interquartile range of the modeled exposure ages. Opdyke et al. (1984) have made similar qualitative observations and interpretations on the Atlantic coast of Northern Florida. There, as is true throughout the Florida panhandle, Pleistocene units overlie older Cenozoic carbonate rocks. Opdyke et al. (1984) conclude that, as a result of karstification of buried carbonates across the Florida peninsula, the region is experiencing epeirogenic uplift associated with the isostatic response to unloading. Models of subsurface and surface dissolution combined with sea level oscillations, past precipitation changes, and crustal evolution and uplift have been used in attempts to refine rates and ages of abandonment of three beach ridges that are progressively higher and presumably older in succession away from the modern coast (Adams et al., 2010). The results of the Adams et al. (2010) model predict uplift rates around 0.04 mm/y (40 m/My) along the Atlantic coast. This result would be consistent with a surface age of 1.6 My in our modeled depth profile. No surface dating has been attempted on the Atlantic Coast beach ridges, so it is possible that measurement of the beach ridge abandonment ages could give uplift rates equal to those along the western margin of the Florida Platform. Relative sea-level reconstructions will be biased by surface uplift (Hawkes, et al. 2016), demonstrating the importance of empirical constrains on regional uplift.

The Citronelle Fm was previously reported as Plio-Pleistocene in origin with very little absolute age control (Schmidt, 1985). At the locality of Alum Bluff, the age of the upland surface from our field site provides a good estimate for the timing of cessation of accumulation for the Citronelle Fm. There is no clear evidence of stratigraphically higher sediments nearby, so the age estimate of ~2 My is an appropriate regional age of formation for the uppermost Citronelle Fm. There is paleontological evidence for Late Pliocene to Pre-Nebraskan Pleistocene ages of lower portions of the Citronelle to the west (Otvos, 1998). This age is not obviously as applicable to eastern exposures, and with little relative age control across its extent, there is no evidence to refute that it might be time-transgressive along the Plio-Pleistocene Gulf coast.

4.4 Numerical limits to the use of the zipper approach

The range of surface conditions over which the approach embodied in Eq. 3 can yield valid results is constrained by the *in-situ* accumulation of nuclides to exclude both very fast and very slow rates of unzipping. The propagation velocity cannot be so high that the accumulated concentrations of nuclides are smaller than methodological uncertainties. Stated differently, any measurable change in concentrations along a gradient must be greater than the methodological uncertainty, which is taken to be a fraction, α, of a measured concentration.

$$\Delta N > \alpha N \tag{7}$$

When combined with Eq. 4, Eq. 7 results in a maximum velocity constraint given by

$$V < \left(\frac{P_0}{N} e^{-\Lambda z} - \lambda\right) \frac{\Delta x}{\alpha} \tag{8}$$

where Δx is the total distance with units of m over which a concentration change is measured. Taking reasonable values for the parameters in Eq. 8, and assuming negligible erosion after unzipping, it is realistic that measurement of topographic features with migration velocities as high as 1 m/y could be achieved. Therefore, this method is appropriate for systems such as migrating knickpoints or retreating ice sheets. In systems where valley walls continue to appreciably erode after unzipping, this upper bound would be lowered owing to the overall decrease in nuclide concentrations that would result.

On the other end of the measurable velocity range, the duration of unzipping over a given distance must be shorter than the time required to reach equilibrium between production and decay of radionuclides.

$$\frac{\Delta x}{V} < \frac{\beta}{\lambda + \Lambda \varepsilon} \tag{9}$$

Here $\Delta x/V$ is the temporal duration with units y over which the gradient along Δx had to accumulate, β is the number of half-lives to a measurable concentration equilibrium, and ε is the erosion of a surface after unzipping. Measurement uncertainty must be accounted for by relating β to the methodological uncertainty. When the concentration is within a fraction α of the equilibrium concentration, the gradient in concentration can no longer grow in time. The number of half-lives necessary to reach this condition is given by

$$-\log_2 \alpha = \beta \tag{10}$$

Combining Eq. 9 with Eq. 10 gives a minimum velocity constraint.

$$V > \frac{(\lambda + \Lambda\epsilon)\Delta x}{-\log_2 \alpha} \tag{11}$$

Substituting reasonable but limiting values into Eq. 11 and assuming negligible erosion subsequent to unzipping, it is possible to attain measurements of topographic features that migrate with velocities as low as 10^{-6} m/y. Continued erosion after unzipping could be a major source of error in locales with low migration velocities, but even with modestly high erosion (10^{-3} m/y), it should still be possible to measure topographic migration rates at 10^{-3} m/y. On this end of the velocity range, it is very likely that this method could be successfully applied to the evolution of passive margin escarpments.

The method introduced here can be equally applied to modern and ancient unzipping processes as long as the above constraints are noted. There is however an additional constraint for processes that have long ceased. In this case accumulation of nuclides would continue after unzipping and that accumulation must not be large enough to overwhelm the gradient in the error of the total concentration. As an example, if a valley opened or a knickpoint migrated and then stopped, the nuclide concentration gradient in the unzipped portions would not change even though the concentrations would increase. As long as the gradient is larger than the uncertainties associated with the accumulation since unzipping, Eq. 4 still holds.

5.0 Conclusions

Horizontal spatial gradients of *in situ* produced cosmogenic nuclide concentrations provide a framework by which the migration rates of topographic features such as knickpoints, canyons, and seepage-based valley heads can be straightforwardly estimated. Migration rates are inversely proportional to magnitudes of spatial concentration gradient along the valley wall and proportional to local production rates corrected for nuclide decay. This method is insensitive to issues associated with inheritance as long as the inherited nuclide concentration is a constant function of space or the inherited component is small compared to any measurable concentration difference. The range of migration velocities that could be captured depends explicitly on magnitudes of measurement uncertainties, and for Earth-surface conditions, is on the order of 10^{-6} m/y to 10^{1} m/y for low production-low velocity locales and high production-high velocity locales, respectively.

This method was applied to a growing seepage network along the Apalachicola River of Florida. Nuclide concentrations were measured from a vertical profile and a valley margin transect. A best-fit exposure age and surface erosion rate for the land surface, derived by modeling the ^{10}Be concentrations in vertical profile, are ~2 My and 10 mm/ky, respectively. The upper and lower quartile of ages constrained for the Citronelle Fm and undifferentiated sediments in the region are 1.7 and 2.5 My respectively. The overall age of the sediments and elevation of the upland surface suggest bounds of 0.027 and 0.038 mm/y on the uplift rate of the Florida Panhandle since the Pleistocene, consistent with uplift modeling for this region (Adams et al. 2010).

The concentration gradient measured along the valley margin produces an estimate of headward growth in the Beaverdam Creek site of approximately 0.025 m/y. Because this rate estimate does not agree with the approximate timing of network formation and its total length, we suggest that headward migration has proceeded irregularly through time with Quaternary climate variations. An alternative interpretation equally in fitting with the data is that the opening of the seepage valley network began just ~160 ky, initiated by drainage evolution in the Apalachicola River.

Acknowledgments, Samples, and Data

We thank D. Mohrig & D. Rothman for support and discussions during development of this work as well as for introducing us to this field area. Work presented here was supported by NSF grant 1848637 awarded to Dr. Jane Willenbring. Data is hosted in the Dryad Repository at doi:10.5061/dryad.bvq83bk8p. All of the data relevant to this manuscript are in Table 1.

References

Abrams, D., A. Lobkovvsky, A. Petroff, K. Straub, B. McElroy, D. Mohrig, A. Kudrolli, and D. Rothman, (2009), Growth laws for channel networks incised by groundwater flow, Nature Geoscience, DOI: 10.1038/NGEO432.

Adams, P.N., Opdyke, N.D., Jaeger, J.M., (2010), Isostatic uplift driven by karstification and sea-level oscillation: Modeling landscape evolution in north Florida. Geology 38, 531–534. https://doi.org/10.1130/G30592.1

Alvarez Zarikian, C.A., P.K. Swart, J.A. Gifford, and P.L. Blackwelder, (2005), Holocene paleohydrology of Little Salt Spring, Florida, based on ostracod assemblages and stable isotopes: Palaeogeography, Palaeoecology, Palaeoclimatology, 225, 134–156.

Balco, G., J. Briner, R. Finkel, J. Rayburn, J. Ridge, and J. Schaefer, (2009), Regional beryllium-10 production rate calibration for late-glacial northeastern North America, Quaternary Geochronology, 4, 93–107.

Balco G., J. Stone, N. Lifton, T. Dunai, (2008), A simple, internally consistent, and easily accessible means of calculating surface exposure ages and erosion rates from Be-10 and Al-26 measurements, Quaternary Geochronology, 3, 174-195.

Benedetti, L., R. Finkel, D. Papanastassiou, G. King, R. Armijo, F.J. Ryerson, D. Farber, and F. Flerit, (2002), Post-glacial slip history of the Sparta fault (Greece) determined by 36Cl cosmogenic dating: evidence for non-periodic earthquakes, Geophys. Res. Lett. 27, doi:10.1029/2001GL014510.

Briner, J., A. Bini, and R. Anderson, (2009), Rapid early Holocene retreat of a Laurentide outlet glacier through and Arctic fjord, Nature Geoscience, 2, 496–499.

Bierman, P., and M. Caffee, (2001), Steady state rates of rock surface erosion and sediment production across the hyperarid Namib desert and the Namibian escarpment, southern Africa, American Journal of Science, 301, 326–358.

Bierman, P., and E. Steig, (1996), Estimating rates of denudation and sediment transport using cosmogenic isotope abundances in sediment, Earth Surface Processes and Landforms, 21, 125–139.

Brown, E.T., R.F. Stallard, M.C. Larsen, G.M. Raisbeck, and F. Yiou, (1995), Denudation rates determined from the accumulation of *in situ*-produced 10 Be in the Luquillo Experimental Forest Puerto Rico. Earth Planet. Sci. Lett. 129, 193–202.

Dunne, T., 1988. Hydrology and mechanics of erosion by subsurface flow, Hydrogeology. Geological Society of America. Boulder, CO.

Granger, D., J. Kirchner, and R. Finkel, (1996), Spatially averaged long-term erosion rates measured from *in-situ* produced cosmogenic nuclides in alluvial sediment, Journal of Geology, 104, 249-257.

Grimm, E.C., G.L. Jacobson Jr., W.A. Watts, B.C.S. Hansen, and K.A. Maasch, (1993), A 50,000-year record of climate oscillations from Florida and its temporal correlation with the Heinrich events. Science 261, 198-200.

Hawkes, A.D., Kemp, A.C., Donnelly, J.P., Horton, B.P., Peltier, W.R., Cahill, N., Hill, D.F., Ashe, E., Alexander, C.R., 2016. Relative sea-level change in northeastern Florida (USA) during the last ~8.0 ka. Quat. Sci. Rev. 142, 90–101. https://doi.org/10.1016/j.quascirev.2016.04.016

Heimsath, A., W. Dietrich, K. Nishiizumi, and R. Finkel, (1997), The soil production function and landscape equilibrium, Nature, 388, 358-361.

Heimsath, A., W. Dietrich, K. Nishiizumi, and R. Finkel, (1999), Cosmogenic nuclides, topography, and the spatial variation of soil depth. Geomorphology, 27, 151-172.

Howard, A. D., (1988) in Sapping Features of the Colorado Plateau: A Comparative Planetary Geology Field Guide 7183, edited by Howard, A. D., R.C. Kochel, and H.E. Holt, NASA Scientific and Technical Information Division.

Hurst, M.D., Rood, D.H., Ellis, M.A., 2017. Controls on the distribution of cosmogenic 10Be across shore platforms. Earth Surf. Dyn. 5, 67–84. https://doi.org/10.5194/esurf-5-67-2017

Jackson, S.T., R. S. Webb, K. H. Anderson, J. T. Overpeck, T. Webb III, J. W. Williams, and B.C.S. Hansen, (2000), Vegetation and environment in Eastern North America during the Last Glacial Maximum, Quaternary Science Reviews, 19, 489–508, doi:10.1016/S0277-3791(99)00093-1.

Jakica, S., Quigley, M.C., Sandiford, M., Clark, D., Fifield, L.K., Alimanovic, A., 2011. Geomorphic and cosmogenic nuclide constraints on escarpment evolution in an intraplate setting, Darling Escarpment, Western Australia. Earth Surf. Process. Landforms 36, 449–459. https://doi.org/10.1002/esp.2058

Jansen, J.D., Fabel, D., Bishop, P., Xu, S., Schnabel, C., Codilean, A.T., 2011. Does decreasing paraglacial sediment supply slow knickpoint retreat? Geology 39, 543–546. https://doi.org/10.1130/G32018.1

Johnson, D.W., 1907. RIVER CAPTURE IN THE TALLULAH DISTRICT, GEORGIA. Science (80-.). 25, 428–432. https://doi.org/10.1126/science.25.637.428-a

Kohl CP and K. Nishiizumi, (1992), Chemical isolation of quartz for measurement of *in-situ*-produced cosmogenic nuclides. Geochim. Cosmochim. Acta, 56, 3583-3587.

Kwit, C., Schwartz, M.W., Platt, W.J., Geaghan, J.P., 1998. The distribution of tree species in steepheads of the Apalachicola River Bluffs, Florida. J. Torrey Bot. Soc. 125, 309–318. https://doi.org/10.2307/2997244

Laîné, A., M. Kageyama, D. Salas-Melia, A. Voldoire, G. Riviere, G. Ramstein, S. Planton, S. Tyteca, and J.Y. Peterschmitt, (2009), Northern Hemisphere storm tracks during the last glacial maximum in the PMIP2 ocean atmosphere coupled models: Energetic study, seasonal cycle, precipitation: Climate Dynamics, 32, 593–614.

Lal, D., (1988), *In situ*-produced cosmogenic isotopes in terrestrial rocks, Annual Reviews Earth Planetary Science, 16, 355-388.

Lal, D., (1991), Cosmic ray labeling of erosion surfaces: *in situ* nuclide production rates and erosion models, Earth and Planetary Science Letters, 104, 424-439.

Laloy, E., Vrugt, J.A., 2012. High-dimensional posterior exploration of hydrologic models using multiple-try DREAM (ZS) and high-performance computing. Water Resour. Res. 48, 1–18. https://doi.org/10.1029/2011WR010608

Laloy, E., Beerten, K., Vanacker, V., Christl, M., Rogiers, B., Wouters, L., 2017. Bayesian inversion of a CRN depth profile to infer Quaternary erosion of the northwestern Campine Plateau (NE Belgium). Earth Surf. Dyn. 5, 331–345. https://doi.org/10.5194/esurf-5-331-2017

Mackey, B.H., Scheingross, J.S., Lamb, M.P., Farley, K.A., 2014. Knickpoint formation, rapid propagation, and landscape response following coastal cliff retreat at the last interglacial sea-level highstand: Kaua'i, Hawai'i. Bull. Geol. Soc. Am. 126, 925–942. https://doi.org/10.1130/B30930.1

Mitchell, S.G., A. Matmon, P.R. Bierman, M. Caffee, and D. Rizzo, (2001), Displacement history of a limestone normal fault scarp, northern Israel, from cosmogenic 36Cl, J.Geophys. Res. 10, 4247– 4264.

Nishiizumi, K., C. Kohl, J. Arnold, J. Klein, D. Fink, and R. Middleton, (1991), Cosmic ray produced 10Be and 26Al in Antarctic rocks: exposure and erosion history, Earth and Planetary Science Letters, 104, 440-454.

Opdyke, N.D., D.P. Spangler, D.L. Smith, D.S. Jones, and R.C. Lindquist, (1984), Origin of the epeirogenic uplift of Pliocene-Pleistocene beach ridges in Florida and development of the Florida karst, Geology, 12, 226–228, doi:10.1130/0091-7613(1984)12<226:OOTEUO>2.0.CO;2.

Otvos, E.G., (1998), Citronelle Formation, northeastern Gulf Coastal Plain; Pliocene stratigraphic framework and age issues, Gulf Coast Association of Geological Societies Transactions, 48, 321–333.

Palumbo, L., L. Benedetti, D. Bourles, A. Cinque, and R. Finkel, (2004), Slip history of the Magnola Fault (Apennines, Central Italy) from 36Cl surface exposure dating: Evidence for strong earthquake over the Holocene, Earth Planet. Sci. Lett., 225, 163–176.

Pelletier, J.D., Taylor Perron, J., 2012. Analytic solution for the morphology of a soil-mantled valley undergoing steady headward growth: Validation using case studies in southeastern Arizona. J. Geophys. Res. Earth Surf. 117, 1–11. https://doi.org/10.1029/2011JF002281

Perron, J.T., Hamon, J.L., 2012. Equilibrium form of horizontally retreating, soil-mantled hillslopes: Model development and application to a groundwater sapping landscape. J. Geophys. Res. Earth Surf. 117. https://doi.org/10.1029/2011JF002139

Petroff, A.P., Devauchelle, O., Abrams, D.M., Lobkovsky, A.E., Kudrolli, A., Rothman, D.H., 2011. Geometry of valley growth. J. Fluid Mech. 673, 245–254. https://doi.org/10.1017/S002211201100053X

Repka, J., R. Anderson, and R. Finkel, (1997), Cosmogenic dating of fluvial terraces, Fremont River, Utah, Earth and Planetary Science Letters, 152, 59-73.

Reusser, L., P. Bierman, M. Pavich, E. Zen, J. Larsen, and R. Finkel, (2004), Rapid Late Pleistocene incision of Atlantic passive margin river gorges, Science, 305, 499-502.

Schmidt, W., (1985), Alum Bluff, Liberty County, Florida, Florida Geological Survey Open File Report No. 9, 11pp.

Schumm, S., K. Boyd, C. Wolff, and W. Spitz, (1995), A ground-water sapping landscape in the Florida Panhandle, Geomorphology, 12, 281-297.

Sepkoski Jr, J.J. and Rex, M.A., (1974), Distribution of freshwater mussels: coastal rivers as biogeographic islands. Systematic Biology, 23(2), 165-188.

Swirad, Z.M., Rosser, N.J., Brain, M.J., Rood, D.H., Hurst, M.D., Wilcken, K.M., Barlow, J., 2020. Cosmogenic exposure dating reveals limited long-term variability in erosion of a rocky coastline. Nat. Commun. 11, 1–9. https://doi.org/10.1038/s41467-020-17611-9

Ter Braak, C.J.F., Vrugt, J.A., 2008. Differential Evolution Markov Chain with snooker updater and fewer chains. Stat. Comput. 18, 435–446. https://doi.org/10.1007/s11222-008-9104-9

Valla, P.G., Van Der Beek, P.A., Lague, D., 2010. Fluvial incision into bedrock: Insights from morphometric analysis and numerical modeling of gorges incising glacial hanging valleys (Western Alps, France). J. Geophys. Res. Earth Surf. 115. https://doi.org/10.1029/2008JF001079

Van Beynen, P. E., L. Soto, and J. Polk, (2008), Variable calcite deposition rates as proxy for paleo-precipitation determination as derived from speleothems in Central Florida, U.S.A. Journal of Cave and Karst Studies, 70, 25–34.

Vanacker, V., F. von Blanckenburg, T. Hewawasam, and P. Kubik, (2007), Constraining landscape development of the Sri Lankan escarpment with cosmogenic nuclides in river sediment, Earth and Planetary Science Letters, 253, 402-414.

von Blankenburg, F., (2006), The control mechanisms of erosion and weathering at basin scale from cosmogenic nuclides in river sediment, Earth and Planetary Science Letters, 237, 462-479.

Vrugt, J.A., ter Braak, C.J.F., Diks, C.G.H., Robinson, B.A., Hyman, J.M., Higdon, D., 2009. Accelerating Markov Chain Monte Carlo Simulation by Differential Evolution with Self-Adaptive Randomized Subspace Sampling. Int. J. Nonlinear Sci. Numer. Simul. 10, 1–4. https://doi.org/10.1515/IJNSNS.2009.10.3.273

Ward, D. J., R. S. Anderson, Z. S. Guido, and J. P. Briner (2009), Numerical modeling of cosmogenic deglaciation records, Front Range and San Juan Mountains, Colorado, J. Geophys. Res., 114, F01026, doi:10.1029/2008JF001057.

Willett, S.D., McCoy, S.W., Perron, J.T., Goren, L., Chen, C.-Y., 2014. Dynamic Reorganization of River Basins. Science (80-.). 343, 1248765–1248765. https://doi.org/10.1126/science.1248765

Zavala, V., Carretier, S., Regard, V., Bonnet, S., Riquelme, R., Choy, S., 2021. Along-Stream Variations in Valley Flank Erosion Rates Measured Using 10Be Concentrations in Colluvial Deposits From Canyons in the Atacama Desert. Geophys. Res. Lett. 48, 1–11. https://doi.org/10.1029/2020GL089961